Hohlraum-Driven Mid-Z (SiO_2) Double-Shell Implosions on the Omega Laser Facility and Their Scaling to NIF

H. F. Robey, P. A. Amendt, J. L. Milovich, H.-S. Park, A. V. Hamza, and M. J. Bono
Lawrence Livermore National Laboratory, Livermore, California 94551, USA
(Received 3 April 2009; published 1 October 2009)

High-convergence, hohlraum-driven implosions of double-shell capsules using mid-Z (SiO_2) inner shells have been performed on the OMEGA laser facility [T. R. Boehly *et al.*, Opt. Commun. **133**, 495 (1997)]. These experiments provide an essential extension of the results of previous low-Z (CH) double-shell implosions [P. A. Amendt *et al.*, Phys. Rev. Lett. **94**, 065004 (2005)] to materials of higher density and atomic number. Analytic modeling, supported by highly resolved 2D numerical simulations, is used to account for the yield degradation due to interfacial atomic mixing. This extended experimental database from OMEGA enables a validation of the mix model, and provides a means for quantitatively assessing the prospects for high-Z double-shell implosions on the National Ignition Facility [Paisner *et al.*, Laser Focus World **30**, 75 (1994)].

DOI: 10.1103/PhysRevLett.103.145003 PACS numbers: 52.57.Fg, 52.57.Bc

Indirectly-driven double-shell (DS) implosions are being investigated as a possible noncryogenic path to ignition on the recently commissioned National Ignition Facility (NIF) [1]. Potential benefits of double-shell targets as compared to the National Ignition Campaign (NIC) point design [2] include room-temperature deuterium-tritium (DT) fuel, reduced laser backscatter in vacuum hohlraums, lower volume-ignition temperatures ($\approx$4 keV), relaxed hohlraum x-ray flux asymmetry tolerances, and minimal shock-timing requirements. On the other hand, double-shell ignition presents several challenges including (1) room-temperature containment of high-pressure DT gas ($\approx$800 atm) in the inner shell, (2) strict concentricity requirements on the two shells (offset <3 μm), (3) development of nanoporous (<100 nm), low-density (<100 mg/cc) metallic foams for structural support of the inner shell and hydrodynamic instability mitigation, and (4) effective control of perturbation growth on the high-Atwood number interface between the DT fuel and the high-Z inner shell [3].

A previous double-shell campaign on the Omega laser using low-Z, polystyrene (CH) inner shells was described in [4]. These implosions were very successful and produced approximately 25% of the calculated two-dimensional (2D) clean yields. DS implosions on NIF, by contrast, would employ high-Z (Au) inner shells to achieve the required radiation confinement, and are expected to experience a significantly greater yield reduction due to the effects of interfacial mixing at the inner shell-fuel interface. In order to bridge this gap and provide a quantitative capability for assessing the effects of mix in NIF-scale double shells, an additional DS campaign has been conducted on the Omega laser using mid-Z (SiO_2) inner shells. The results of these experiments are presented in this Letter.

An analytic model that accounts for the growth of Richtmyer-Meshkov (RM) [5,6] and Rayleigh-Taylor (RT) [7,8] instabilities at the inner-shell-fuel interface is also presented. The model is validated by comparison to highly resolved 2D simulations using the radiation hydrodynamics code HYDRA [9]. Inclusion of the effect of mix brings the predicted neutron yields to within 30%–40% of the measured values for both sets of Omega implosions and, more importantly, predicts the possibility of successful ignition for a DS implosion on NIF.

The capsules for the present experiments consisted of an 8 μm SiO_2 inner shell with an outer radius of 111 μm, a material-matching, low-density intrashell SiO_2 foam layer of density 50 ± 5 mg/cc, and a 53 μm 2% bromine-doped CH (polystyrene) outer shell with an outer radius of 275 μm. The deuterium fuel pressure was 62 ± 1 atm. These capsules build on results of earlier double-shell experiments reported in [10], but differ in several impor-

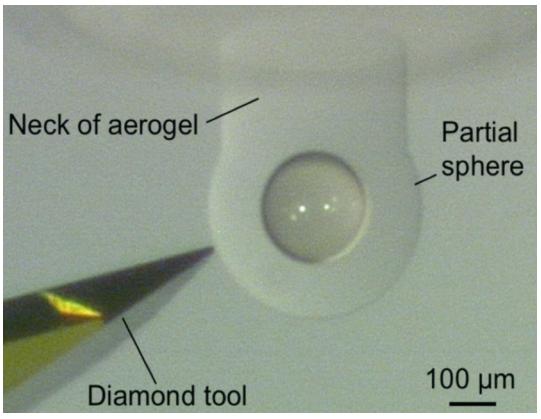

FIG. 1 (color online). Photograph of an inner shell cast in a seamless block of aerogel foam during machining of the foam sphere.

tant regards. A Br-doped ablator is consistently used in both the CH and SiO_2 capsules to reduce the effect of M-band radiation on the inner shell. This was found to improve the performance of a subset of DS implosions in [10], and a similar Cu-doped Beryllium ablator will be used on NIF. The inner shells in the present experiments are approximately 3 times thinner, however, than those used in [10], providing improved fall-line performance [1], which enables a neutron yield that is dominated ($>99\%$) by fuel compression as opposed to shock stagnation as is required for successful DS ignition. Finally, both the CH and SiO_2 capsules employ the same material for the inner shell and foam stages to minimize instability at this interface. This instability reduction technique is also planned for NIF ignition DS implosions [11].

Advances continue to be made in target fabrication to improve the repeatability of DS performance [12]. Figure 1 shows a photograph of an inner shell seamlessly cast into a block of aerogel foam, which was subsequently machined to produce a single, spherically symmetric component. Previous DS capsules employed a pair of machined hemispherical foam shells, which introduced machining perturbations at the inner shell-foam interface and allowed for the possibility of misalignment. The quality of the surrounding ablator has also been improved, with the gap in the step joint of the ablator hemispherical shells reduced from 2 μm for the previous CH DS to better than 0.4 μm for the SiO_2 DS targets. Radial offsets between the two ablator halves have also been reduced from as large as 2.5 μm (CH) to better than 0.5 μm for the present SiO_2 DS.

The experiments were fielded in cylindrical Au hohlraums (2500 μm $\times$ 1600 μm diameter) with a 75% laser entrance hole using 40 beams of the Omega laser at the Laboratory for Laser Energetics (LLE). A dedicated characterization of the UV transmission through the debris shields was conducted by the LLE just prior to the shot day to give the best possible characterization of the on-target laser energy. The pulse shape was a 2.3 ns reverse ramp with a total 3ω energy of 13.4 ± 0.4 kJ (shot-to-shot variation), designed to produce a nearly constant radiation temperature T_R in the hohlraum.

A wide range of experimental diagnostics was employed on these shots. In addition to the primary diagnostics measuring neutron yield, a number of x-ray diagnostics were fielded to characterize the implosions and benchmark numerical simulations. Figure 2 shows the radiation temperature history measured by Dante, a 12-channel array of filtered, calibrated x-ray diodes. The agreement in T_R between experiment and simulation is quite good. The hard x-ray preheat used in the simulations was adjusted to match the measured nonthermal gold M-band component (2–4 keV). Additional information was provided by time-gated x-ray images of the implosion. Figure 3 shows a series of 3 (of 16) backlit x-ray images at an energy of 4.3 keV obtained by directing an additional 7 beams onto a 5 μm thick Sc foil positioned over a 400 μm diameter

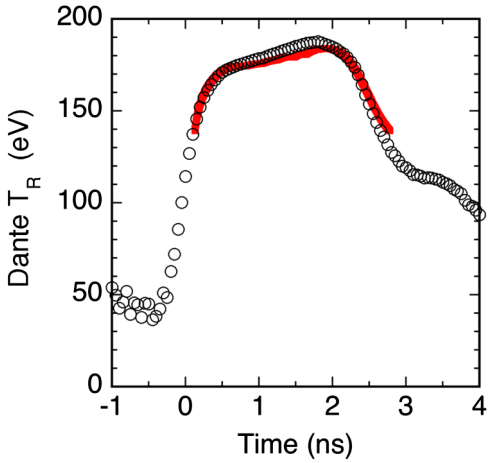

FIG. 2 (color online). Comparison between the experimentally measured radiation drive (black) with numerical simulations (red).

aperture in the hohlraum wall. Images of the implosion are shown at times 2.47, 2.81, and 3.17 ns, revealing a number of features. The outer boundary of the images is defined by the limiting aperture in the hohlraum wall. At the times shown, the inner shell and the highly compressed surrounding foam have merged and are seen as the dark central feature due to the strong absorption of the backlighter x rays by the SiO_2. A portion of the ablator is also seen in the images. The inner edge of the ablator is heated by conduction from the hotter foam, and the backlighter transmission through this region of locally reduced density is seen as the bright ring surrounding the inner shell. This higher transmission region is due to reduced absorption (and not emission) as confirmed by shots without a backlighter, where emission is observed only from the capsule center. This interface between the ablator and the foam

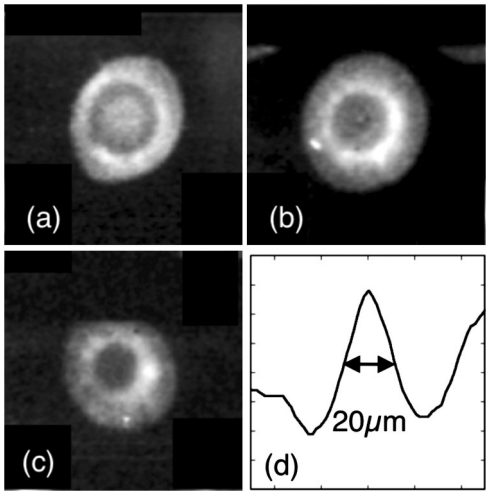

FIG. 3. Temporally-gated backlit x-ray images of the imploding SiO_2 inner shell and foam at (a) $t = 2.47$ ns, (b) $t = 2.81$ ns, and (c) $t = 3.17$ ns. (d) Horizontal lineout of the emission over the central 100 μm from 3(b).

reveals considerable modulation due to instability. By contrast, no such modulation was observed in the previous CH DS implosions, as that ablator-foam interface is much more stable (Atwood number lower by a factor of 4) due to a greater degree of material matching.

The contrast between the dark SiO_2 inner shell-foam material and the bright inner edge of the ablator enables a measurement of the trajectory of the foam-ablator interface vs time. The same procedure was used to define this edge from both the experimental and the simulated radiographs. A comparison of the measured (black) vs simulated (red) trajectories is shown in Fig. 4. The agreement is generally within the ± 10 μm resolution set by the 20 μm imaging pinholes. Also seen in Fig. 3(b) is emission at the capsule center (from the hot inner surface of the SiO_2 shell), which gives a measure of the x-ray bang time. A lineout of this emission over the central 100 μm is shown in Fig. 3(d). The FWHM of the emission profile is 20 μm. The x-ray bang time extracted from the simulations is 2.9 ns—in very good agreement with that measured in the experiments. The combined agreement between experiment and simulation on the radiation drive (Dante) as well as the implosion history (x-ray interface trajectory and x-ray bang time) serves to benchmark the simulations.

The primary experimental diagnostic is the neutron yield. Figure 5 shows a comparison between the measured yield and the 2D simulated yield for both the CH (open symbols) and SiO_2 (solid symbols) DS. The 2D yield is obtained from integrated hohlraum simulations, which include measured differences in laser energy entering each laser entrance hole. For the present experiments, the 2D yield is 40% of the clean 1D yield. Corresponding simulations for 1 and 2 MJ laser energy NIF double shells [11], which use rugby-shaped hohlraums, predict the 2D yields to be 70% and 90% of the 1D values, respectively. The blue solid and open squares give the 2D clean yield for each capsule type. As is seen from the reference curves, the measured yield over clean ranges from 15%–30% for the CH DS and 5%–15% for the SiO_2 DS. We attribute the bulk of this difference between measurement and simulation for both capsule types to the effect of mixing at the inner shell-fuel interface, which we now quantify.

The extent of mix at this interface can be approximated analytically as an RM phase beginning at shock passage followed by a self-similar RT phase commencing at deceleration onset. Note that this simple analysis neglects any contribution from feedthrough of perturbations, which may have grown on the outer surface of the inner shell. The assumption of self-similarity for the RT growth phase is based upon an estimate of the Reynolds number of the mixing layer (see details in [13]), which increases very quickly to a value of 7×10^4. This exceeds the threshold of 2×10^4 given in [14] required for the formation of an inertial subrange and the corresponding transition to a state of significantly increased turbulent mixing. The RM growth is estimated analytically for the bubbles and spikes based on a linear growth-factor analysis, which includes the stabilizing effects of viscosity and mass diffusion (see details in [13]). At deceleration onset, the RM growth results in a root-mean-square bubble-to-spike amplitude $2h_0 = 0.3$ μm (CH) and 0.5 μm (SiO_2). These values are used as the initial mixing layer thickness for the subsequent self-similar RT growth phase. The RT mix width $h(t)$ is then given by [15,16]]

$$h(t) = \alpha A g t^2 + 2(\alpha A g h_0)^{1/2} t + h_0 \qquad (1)$$

where the bubble and spike amplitudes are again calculated separately with $\alpha_B = 0.05$ and α_S taken from the density-dependent expression of Ref. [17]. Here, $A(t)$ and $g(t)$ are

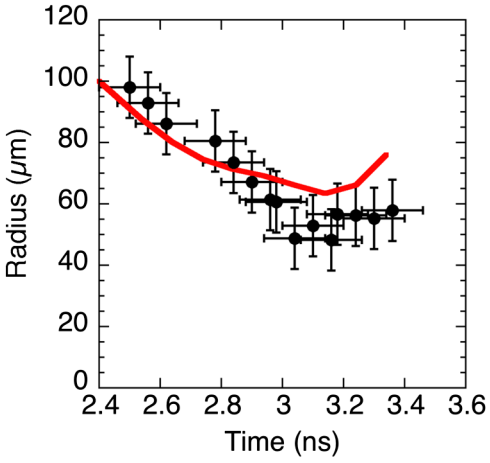

FIG. 4 (color online). (r, t) trajectory of the outer edge of the SiO_2 foam extracted from the gated x-ray images of Fig. 3. The corresponding trajectory obtained from an identical post-processing of the simulated radiographs is shown in red.

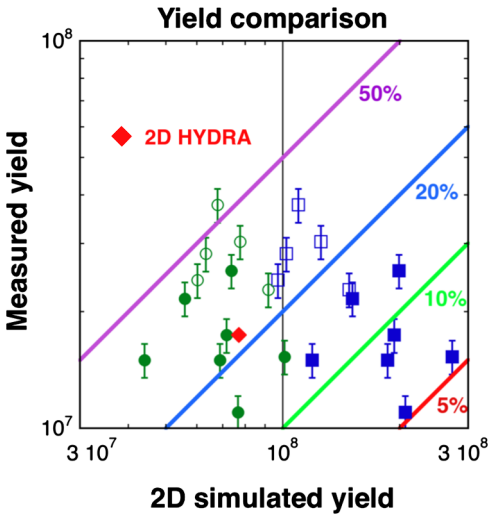

FIG. 5 (color online). Comparison between experimentally measured neutron yield and the 2D simulated clean yield (blue solid and open squares) and an estimate of the yield degradation due to mix at the inner shell-fuel interface (green solid and open circles). Open symbols are for CH inner shells and solid symbols are for SiO_2 inner shells.

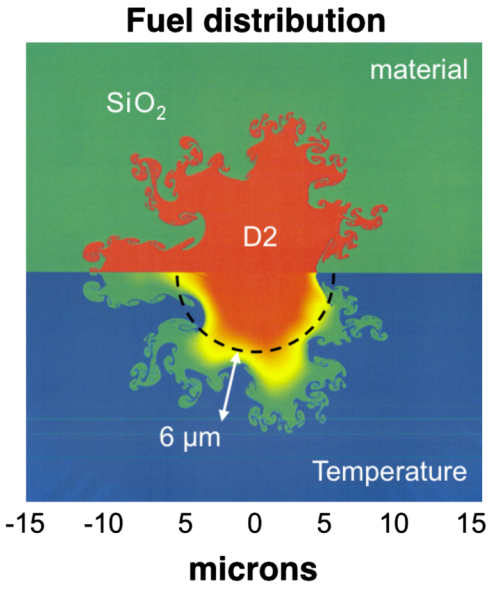

FIG. 6 (color online). Spatial distribution of the deuterium fuel at the time of peak neutron production. Top half plots material distribution, lower half shows temperature distribution of the burning fuel. Dashed curve is the effective radius of the burn region, which is reduced due to mix.

the time-dependent Atwood number and deceleration histories taken from 1D simulations. At the time of peak neutron production, the total mix width at this interface is approximately 3.6 μm (CH) and 6 μm (SiO_2).

This estimate of the mix width can be used to account for a substantial portion of the difference in yield that is observed between the clean 2D simulations and experiment in Fig. 5 (all blue solid and open squares). If the volume of the burning fuel is limited to the unmixed region only, then the simulated yield is reduced from the clean values to the mix-degraded values given by the green solid and open circles in Fig. 5. This mix-degraded "yield over clean" now ranges from 25%–50% (CH) and 15%–40% (SiO_2). As expected, the effect of mix is much more significant for the SiO_2 DS, reducing the predicted value by 63% vs 36% for the CH. A number of phenomena including 3D effects, feedthrough of perturbations from outer interfaces, and the possibility of interfacial plasma effects (ionization gradients and self-generated electric fields) [18] may account for this remaining difference between the mix-degraded simulated yield and the measured values.

These 1D analytic estimates of mixing are consistent with 2D HYDRA simulations that resolve perturbations on all interfaces. The measured spectra of surface roughness for each shell are used. The simulations use 740 radial zones by 4080 azimuthal zones over 180° of the capsule. Initial perturbation scales are resolved down to 1.5 μm on the inner shell, with at least 20 zones resolving the shortest wavelength. Figure 6 shows the resulting distribution of the deuterium fuel at the time of peak neutron production in the SiO_2 DS. The materials are shown on the top, and the temperature of the burning fuel is given on the bottom. As can be seen from the dashed line in Fig. 6, the mix width is very comparable to the 6 μm extent that was estimated analytically with input from 1D parameter histories. The spatial reduction in the effective radius of the burning region lends support to the simple model used above to assess the yield degradation due to mix. The neutron yield from this simulation is 7×10^7. The red solid diamond in Fig. 5 shows this to be in excellent agreement with the average of the mix-degraded yield predictions.

This comparison over two sets of DS implosions with inner shells of different density and atomic number establishes a methodology for extending these results to higher-Z inner shells, which will include increased effects of radiation confinement, and ultimately to potential ignition double shells for the NIF. Indeed, application of this mix model to a recent DS ignition target design [11] predicts a substantial yield reduction (87%) due to mix. The resulting mix-degraded yield prediction for these targets is now 1.1 MJ, which still exceeds the threshold for ignition, and increases our confidence in the prospects for DS ignition. Methods to reduce the susceptibility to performance-degrading mix for higher yield DS implosions are under development.

[1] P. Amendt *et al.*, Phys. Plasmas **9**, 2221 (2002).
[2] D. S. Clark *et al.*, Phys. Plasmas **15**, 056305 (2008).
[3] J. L. Milovich, P. Amendt, M. Marinak, and H. Robey, Phys. Plasmas **11**, 1552 (2004).
[4] P. Amendt *et al.*, Phys. Rev. Lett. **94**, 065004 (2005).
[5] R. D. Richtmyer, Commun. Pure Appl. Math. **13**, 297 (1960).
[6] E. E. Meshkov, Izv. Akad. Nauk. SSSR, Mekh. Zhidk. Gaza **4**, 151 (1969) [Fluid Dynamics **4**, 101 (1969)].
[7] Lord Rayleigh, Proc. London Math. Soc. **14**, 170 (1882); [*Scientific Papers*, (Cambridge University Press, Cambridge, England, 1900) Vol. II, p. 200].
[8] G. I. Taylor, Proc. R. Soc. A **201**, 192 (1950).
[9] M. M. Marinak *et al.*, Phys. Plasmas **8**, 2275 (2001).
[10] W. S. Varnum *et al.*, Phys. Rev. Lett. **84**, 5153 (2000).
[11] P. Amendt *et al.*, Phys. Plasmas **14**, 056312 (2007).
[12] M. Bono *et al.*, Fusion Sci. Technol. **51**, 611 (2007).
[13] H. F. Robey, Phys. Plasmas (to be published).
[14] P. E. Dimotakis, J. Fluid Mech. **409**, 69 (2000).
[15] A. W. Cook, W. Cabot, and P. L. Miller, J. Fluid Mech. **511**, 333 (2004).
[16] J. R. Ristorcelli and T. T. Clark, J. Fluid Mech. **507**, 213 (2004).
[17] G. Dimonte and M. Schneider, Phys. Fluids **12**, 304 (2000).
[18] P. Amendt, Phys. Rev. Lett. **101**, 115004 (2008).